Mid-infrared laser measurements of aqueous glucose

Bujin Guo*
Yi Wang*
Yang Wang
Han Q. Le
University of Houston
Photonic Device and System Laboratory
Department of Electrical and Computer Engineering
and
Texas Center for Advanced Materials and Southwest
Public Safety Technology Center
4800 Calhoun
Houston, Texas 77204
E-mail: hqle@uh.edu

Abstract. Mid-IR semiconductor lasers of two wavelength bands, 5.4 and 9.6 μm, are applied to measure aqueous glucose concentration ranging from 0 to 500 mg/dL with Intralipid® emulsion (0 to 8%) added as a fat simulator. The absorption coefficient μ_a is found linear with respect to glucose and Intralipid® concentrations, and their specific absorption coefficients are obtained via linear regression. These coefficients are subsequently used to infer the concentrations and compare with known values. The objective is to evaluate the method accuracy. Glucose concentration is determined within ±21 mg/dL with 90% confidence and ±32 mg/dL with 99% confidence, using <1-mJ laser energy. It is limited by the apparatus mechanical error and not the photometric system noise. The expected uncertainties due to photometric noise are ±6 and ±9 mg/dL with 90 and 99% confidence, respectively. The uncertainty is fully accounted for by the system intrinsic errors, allowing rigorous inference of the confidence level. Intralipid® is found to have no measurable effect on glucose determination. Further analysis suggests that a few mid-IR wavelengths may be sufficient, and that the laser technique offers advantages with regard to accuracy, speed, and sample volume, which can be small, $\sim 0.4 \times 10^{-7}$ mL for applications such as microfluidic or microbioarray monitoring. [DOI: 10.1117/1.2714283]

Keywords: glucose; laser glucose measurement; mid-infrared laser spectroscopy.

Paper 06129RR received May 19, 2006; revised manuscript received Jan. 4, 2007; accepted for publication Jan. 4, 2007; published online Apr. 13, 2007.

1 Introduction

There have been extensive efforts to develop optical techniques to measure blood glucose concentration for diabetes care.[1–3] There is also the application of *in situ* real-time monitoring of glucose in cell culture, microassay arrays, and bioreactors. In both applications, accuracy, reliability, and speed are important. This work is about a laser-based photometric technique that can address these issues. This work aims primarily for the latter application, but the technique is potentially applicable for blood glucose.

A broad review of minimally or noninvasive blood glucose monitoring has been given by Klonoff.[4] More recently, Khalil[5] and Cote[6] specifically reviewed optical spectroscopy, including absorption, polarimetry, Raman, and fluorescence. Absorption spectroscopy in particular, for both the near-IR (NIR) and mid-IR (MIR) spectral region, has been explored extensively by many research groups and commercial concerns over many years.[7–24] For the MIR "fingerprint" region, Heise et al.[7] in early work[7] analyzed blood glucose *in vitro* using Fourier transform infrared (FTIR) spectroscopy. Bhandare et al.[9] also used FTIR to investigate the spectral interference of other blood constituents on the glucose signature. In more recent works,[10–13] various groups focused on using only a few key MIR wavelengths rather than the entire spectrum to determine blood glucose. Specifically, Shen et al.[11] found that spectroscopy at just two wavenumbers, 1082 and 1093 cm^{-1}, was sufficient. Rhiel et al.[14] employed FTIR to monitor not only glucose but also lactose and ammonia in cell culture in real time. Opposite to absorption, MIR radiation was also used to measure glucose based on Kirchoff's law of thermal emission.[15] Some other works are based on laser photoacoustic effects.[25,26]

There are generally three aspects in these studies: the spectroscopy aspect is concerned with spectral features and processing algorithms; the photometry aspect is concerned with optical system engineering and measurements; and the deployment aspect is concerned with application. Photometry is often undervalued and underdeveloped compared to spectroscopy but essential for real-life applications. The MIR works,[7–15] for example, demonstrated the spectroscopic merit, but the photometry was simply lacking. The thermal-source FTIR instrument employed in these works is useful as a research instrument but not necessarily practical or cost effective. Thermal sources have low power spectral density, low radiance, high relative intensity noise (RIN), and large $1/f$ thermal noise. These impose limitations on dynamic range and speed for accuracy and real-time monitoring. In comparison, the NIR approach does not have any intrinsic spectro-

*Current affiliation: AOI, Sugar Land, TX.
Address all correspondence to Han Q. Le, University of Houston, 4800 Calhoun, Department of Electrical Engineering, Houston, TX 77204. Tel: 713–743–4465; Fax: 713–743–4402; E-mail: hqle@uh.edu

1083-3668/2007/12(2)/024005/14/$25.00 © 2007 SPIE

scopic advantage, but benefits greatly from more advanced photometric technologies.

Recent progress can help exploit the MIR region. This work describes the use of advanced MIR semiconductor lasers for *in vitro* aqueous glucose measurements. Lasers have well-established photometric advantages including high spectral intensity, brightness, high modulation bandwidth, low RIN, and $1/f$ noise. They are also well suited for applications such as microfluidic or microarray bioassay, as the beam can be focused to a small volume. For practicality, they are robust, compact, and potentially low cost. Advanced MIR semiconductor lasers have been demonstrated for tissue imaging,[27] and application for conjunctiva glucose measurement is being developed.[24] A potential issue with MIR lasers is the lack of large spectral coverage, but some studies have shown that only a few wavelengths may be needed.[11,13,24] Also, recent progress in tunable MIR lasers[27–31] promises broad wavelength coverage.

Photometry is crucial to the issue of accuracy. There is often some ambiguity on what contributes to glucose measurement errors: how much it is due to spectroscopic problems (interference, distorted spectra, etc.), and how much is due to photometric errors. Glucose errors were usually determined by comparing with wet chemistry results, but not analytically linked to instrument performance. As a basic principle of system engineering, a system should fully account for all errors, and establish an intrinsic measurement confidence level based on the causal and deterministic relation with the instrument noises and errors. This is a focus of this work.

The experiments were performed for glucose in water and Intralipid® (IL) solution. It is chemically much simpler than blood, since the objective is to establish the baseline photometric merit without the issue of chemical complexity. It is hoped that it may eventually motivate blood applications with many-wavelength systems to handle the chemical complexity. The rest of the work is organized as follows. Section 2 describes the experimental approach. Results and discussion are presented in Sec. 3; and Sec. 4 presents a summary and conclusion.

2 Experimental approach

2.1 *Overall Concept*

2.1.1 *Regression Approach*

Given a glucose solution with concentration C_{glu}, which also contains an interferent substance such as IL of concentration C_{IL}, a system can determine these concentrations via the equation:

$$\begin{pmatrix} \hat{C}_{\text{glu}} \\ \hat{C}_{\text{IL}} \end{pmatrix} = \begin{pmatrix} q_{\text{glu},1} & q_{\text{glu},2} & \cdots & q_{\text{glu},n} \\ q_{\text{IL},1} & q_{\text{IL},2} & \cdots & q_{\text{IL},n} \end{pmatrix} \cdot \begin{bmatrix} \Delta\mu_a(\lambda_1) \\ \Delta\mu_a(\lambda_2) \\ \vdots \\ \Delta\mu_a(\lambda_n) \end{bmatrix} + \text{higher order terms}, \tag{1}$$

where $\Delta\mu_a(\lambda_n)$ is the difference between the absorption coefficient of the solution and that of pure water $\Delta\mu_a(\lambda) \equiv \mu_{a,\text{solution}}(\lambda) - \mu_{a,\text{water}}(\lambda)$, and coefficients q are quantities to be obtained from calibration. For glucose and IL solution, it is expected that $\mu_a \gg \mu_s$ in the MIR owing to Rayleigh's λ^{-4} scattering law and the latter can be neglected. In Eq. (1), it is seen that higher-order terms are negligible; and it is convenient to use the matrix format:

$$\hat{\mathbf{C}} = \mathbf{Q} \cdot \Delta\boldsymbol{\mu}_a, \tag{2}$$

where the notation $\hat{C}$ indicates that it is only an inferred estimate of the true value C. In more complex solutions with k substances, $\hat{\mathbf{C}}$ would represent k values of concentration.

The calibration for $\mathbf{Q}$ is obtained from $\Delta\mu_a(\lambda)$ measured for solutions of known $C_{\text{glu}}^{\text{cal}}$ and $C_{\text{IL}}^{\text{cal}}$ based on the relation:

$$\begin{aligned} \Delta\mu_a(\lambda) &\equiv \mu_a(\lambda; C_{\text{glu}}^{\text{cal}}, C_{\text{IL}}^{\text{cal}}) - \mu_a(\lambda; 0, 0) \\ &= \sigma_{a,\text{glu}}(\lambda) C_{\text{glu}}^{\text{cal}} + \sigma_{a,\text{IL}}(\lambda) C_{\text{IL}}^{\text{cal}} \\ &\quad + \text{higher-order terms}(C_{\text{glu}}^{\text{cal}^2} C_{\text{IL}}^{\text{cal}^2}, C_{\text{glu}}^{\text{cal}} C_{\text{IL}}^{\text{cal}}, \cdots), \end{aligned} \tag{3}$$

where superscript "cal" indicates that these are calibrated concentrations, and $\sigma_{a,\text{glu/IL}}(\lambda)$ is the specific absorption coefficient. As it turns out, all higher-order nonlinear terms were found insignificant and the relation becomes:

$$\Delta\boldsymbol{\mu}_a^{\text{cal}} = \boldsymbol{\Sigma} \cdot \mathbf{C}^{\text{cal}}, \tag{4}$$

where:

$$\Delta\boldsymbol{\mu}_a^{\text{cal}} = \begin{pmatrix} \Delta\mu_{a,1}(\lambda_1) & \Delta\mu_{a,2}(\lambda_1) & \cdots & \Delta\mu_{a,p}(\lambda_1) \\ \Delta\mu_{a,1}(\lambda_2) & \Delta\mu_{a,2}(\lambda_2) & \cdots & \Delta\mu_{a,p}(\lambda_2) \\ \vdots & \vdots & \ddots & \vdots \\ \Delta\mu_{a,1}(\lambda_n) & \Delta\mu_{a,2}(\lambda_n) & \cdots & \Delta\mu_{a,p}(\lambda_n) \end{pmatrix}, \quad \text{and} \tag{5}$$

$$\boldsymbol{\Sigma} = \begin{pmatrix} \sigma_{\text{a,glu}}(\lambda_1) & \sigma_{\text{a,IL}}(\lambda_1) \\ \sigma_{\text{a,glu}}(\lambda_2) & \sigma_{\text{a,IL}}(\lambda_2) \\ \vdots & \vdots \\ \sigma_{\text{a,glu}}(\lambda_n) & \sigma_{\text{a,IL}}(\lambda_n) \end{pmatrix}, \tag{6}$$

$$\mathbf{C}^{\text{cal}} = \begin{pmatrix} C_{1,\text{glu}}^{\text{cal}} & C_{2,\text{glu}}^{\text{cal}} & \cdots & C_{p,\text{glu}}^{\text{cal}} \\ C_{1,\text{IL}}^{\text{cal}} & C_{2,\text{IL}}^{\text{cal}} & \cdots & C_{p,\text{IL}}^{\text{cal}} \end{pmatrix},$$

where p is the number of calibrated samples. With linear regression, the estimate for $\boldsymbol{\Sigma}$ is:

$$\hat{\Sigma} = \Delta\boldsymbol{\mu}_a^{\text{cal}} \mathbf{C}^{\text{cal}^{\text{T}}} (\mathbf{C}^{\text{cal}} \mathbf{C}^{\text{cal}^{\text{T}}})^{-1}. \tag{7}$$

The relation between $\mathbf{Q}$ and $\boldsymbol{\Sigma}$ is simply: $\mathbf{Q} = (\boldsymbol{\Sigma}^{\text{T}}\boldsymbol{\Sigma})^{-1}\boldsymbol{\Sigma}^{\text{T}}$ and Eq. (2) becomes:

$$\hat{\mathbf{C}} = (\boldsymbol{\Sigma}^{\text{T}}\boldsymbol{\Sigma})^{-1}\boldsymbol{\Sigma}^{\text{T}} \cdot \Delta\boldsymbol{\mu}_a. \tag{8}$$

2.1.2 *Uncertainty and confidence level analysis*

The critical issue and an objective of this work is the confidence level of $\hat{\mathbf{C}}$. Mathematically, it is a function of two independent random variables $\Delta\boldsymbol{\mu}_a$ and $\boldsymbol{\Sigma}$. The error of $\Delta\boldsymbol{\mu}_a$ is

based on the photometric system: laser, detector, electronic noises, and other measurement apparatus errors. $\boldsymbol{\Sigma}$ is a random variable not in the sense that it varies from one measurement to the next, but that it has an intrinsic uncertainty associated from imperfect calibration.

Ideally, if $\boldsymbol{\Sigma}$ is very accurately calibrated, the uncertainty of $\hat{\mathbf{C}}$ was caused only by photometric measurement error. In this case, $\Delta\boldsymbol{\mu}_a$ error can be characterized by a normal distribution $N(0,\delta)$. Then, $\mathbf{C}$ is also a normal distribution function with an estimated variance:

$$\text{variance}(\mathbf{C}) = (\boldsymbol{\Sigma}^{\mathrm{T}}\boldsymbol{\Sigma})^{-1}\delta^2; \quad \text{or variance}(C_i) = (\boldsymbol{\Sigma}^{\mathrm{T}}\boldsymbol{\Sigma})^{-1}_{ii}\delta^2. \tag{9}$$

Realistically however, there is no perfect calibration and this is a key issue for optical glucose technologies. Calibration may have to be done frequently, as it can be unique to an individual or apparatus and can change over time. The expected variance of $\boldsymbol{\Sigma}$ from Eq. (7) is:

$$\text{variance}(\boldsymbol{\Sigma}) = (\mathbf{C}^{\text{cal}}\mathbf{C}^{\text{cal}^{\mathrm{T}}})^{-1}\text{variance}(\Delta\boldsymbol{\mu}_a^{\text{cal}}), \tag{10}$$

which also depends on $\Delta\boldsymbol{\mu}_a^{\text{cal}}$ photometric error, though it is not necessarily the same as that in Eq. (9). Photometry thus has a two-fold impact on error, and the quality of calibration is critical.

With $\boldsymbol{\Sigma}$ uncertainty taken into account, the uncertainty of $\mathbf{C}$ can then be complex, and variance can be a useless concept. For example, consider the simplest case when $\boldsymbol{\Sigma}$ is a normal-distribution scalar with mean $\hat{\sigma}$ and standard of deviation u; the probability density function (PDF) of C of Eq. (8) is then:

$$\begin{aligned}\text{PDF}(C) = {} & \frac{u\delta}{\pi(\delta^2+C^2u^2)}\exp\left[-\frac{1}{2}\left(\frac{\Delta\mu^2}{\delta^2}+\frac{\hat{\sigma}^2}{u^2}\right)\right] \\ & + \frac{\hat{\sigma}(\delta^2+C\hat{C}u^2)}{\sqrt{2\pi}(\delta^2+C^2u^2)^{3/2}}\exp\left[-\frac{(C-\hat{C})^2}{2(\delta^2+C^2u^2)/\hat{\sigma}^2}\right] \\ & \times\text{erf}\left\{\frac{\hat{\sigma}(\delta^2+C\hat{C}u^2)}{u\delta[2\pi(\delta^2+C^2u^2)]^{1/2}}\right\},\end{aligned} \tag{11}$$

which has an infinite variance owing to the well-known Cauchy tail $\sim 1/C^2$ at large C. Instead of variance, a rigorous measure is the confidence interval, e.g., the interval $[\hat{C}-a/2,\hat{C}+a/2]$ given by equation

$$\int_{\hat{C}-a/2}^{\hat{C}+a/2}\text{PDF}(C)dC = 0.99,$$

which has a 99% probability of containing the true value of glucose concentration.

If $\boldsymbol{\Sigma}$ uncertainties u_{ij} are small: $\max(u_{ij})/\|\boldsymbol{\Sigma}\| \ll 1$, a cutoff can be imposed to keep only the Gaussian component and an approximated variance can be used:

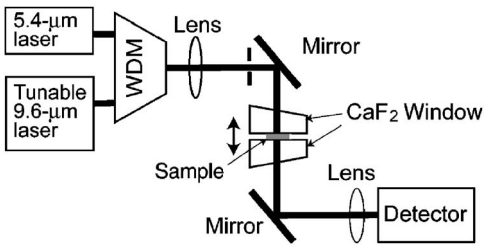

Fig. 1 Block diagram of the glucose measurement apparatus. The lasers are wavelength-division multiplexed and focused on the liquid sample held between two optical windows with adjustable gap.

$$\text{variance}(\mathbf{C}) \approx (\boldsymbol{\Sigma}^{\mathrm{T}}\boldsymbol{\Sigma})^{-1}\delta^2\left[\mathbf{I}+\frac{\overline{\Delta\mu_a}^2}{\delta^2}u^2(\boldsymbol{\Sigma}^{\mathrm{T}}\boldsymbol{\Sigma})^{-1}\right], \tag{12}$$

where $u=\max(u_{ij})$. The uncertainty of $\mathbf{C}$ is degraded from Eq. (9) by an extra term $(\overline{\Delta\mu_a}^2/\delta^2)u^2(\boldsymbol{\Sigma}^{\mathrm{T}}\boldsymbol{\Sigma})^{-1}$, where $\overline{\Delta\mu_a}^2$ is $\Delta\mu_a$ mean square. The simple and intuitively obvious implication of Eq. (12) is that for any system, there is no need to measure $\Delta\boldsymbol{\mu}_a$ with much less error than that of $\boldsymbol{\Sigma}$ and vice versa. More importantly, $\boldsymbol{\Sigma}$ is essentially a spectrum, and arbitrary applications of techniques such as spectral smoothing and other digital filtering, while producing appealing-looking calibration spectra, violates its integrity and may induce spectral distortion that affects the confidence of $\hat{\mathbf{C}}$. A merit and objective of laser-based photometry is to obtain $\hat{\boldsymbol{\Sigma}}$ and $\hat{\mathbf{C}}$ with high confidence that is causally and rigorously linked to the system performance.

2.2 *Experimental Setup*

2.2.1 *Optical configuration and experimental condition*

The experiments were set up to measure sample absorption in the transmission mode, using a tunable MIR semiconductor lasers around 9.6 μm ($\sim$1040 cm^{-1}) and a reference laser at 5.4 μm ($\sim$1850 cm^{-1}). A schematic diagram is shown in Fig. 1. The sample is a thin liquid film held between two CaF_2 windows by surface tension. One window is fixed, and the other is movable with to a stepping-motor-driven micrometer. The sample thickness was varied 50 to 250 μm. The laser beam was focused to a spot $\sim$100 μm diameter. The sample volume was $\sim 0.4-2\times10^{-6}$ mL, which is in the range for microassay or microfluidic applications.

The sample temperature was not measured, but the room temperature was controlled at $\sim 25\pm0.5\,^{\circ}$C. Owing to very low laser power (compare Sec. 2.2.3), the instantaneous temperature rise due to laser adiabatic heating is calculated to be $\sim$0.01 K, and the steady-state average temperature rise is $<$0.005 K (based on water-specific heat of 4.186 J/g K and conductivity of 0.58 W/m K). Thus, the laser-induced temperature rise is insignificant compared to the room temperature fluctuation. There was no effort to study temperature-dependence absorption.

2.2.2 *Sample preparation*

The anhydrous glucose (Avocado Research Chemicals, Heysham, England) was used to prepare the glucose deionized water (DI) water solution samples. Glucose concentrations

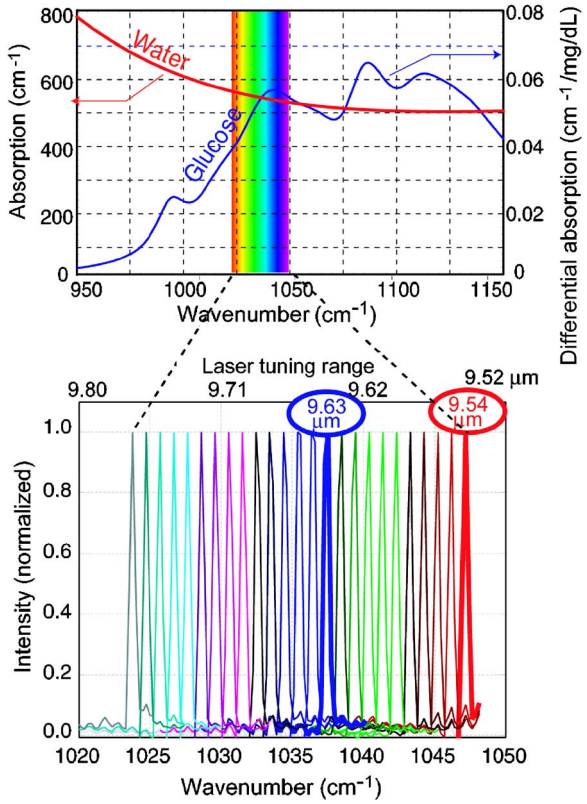

Fig. 2 Top: Glucose absorption spectra in the 9-μm region. Bottom: Spectral output of the tunable laser used in the experiments.

ranged from 0 to 500 mg/dL. The Intralipid® solution of 10% (Baxter, Deerfield, Illinois) was diluted by DI water and mixed with stock glucose solution. The uncertainty of glucose concentration was calculated to be ~1.5 mg/dL based on the errors of glucose weight and water volume measurement. Intralipid® concentration estimated uncertainty was ±0.1%, based on errors of measured liquid volume for mixing.

2.2.3 *Laser and detector*

The MIR tunable laser was operated in single mode, covering from 9.5 to 9.8 μm (1020 to 1050 cm^{-1}) as illustrated in Fig. 2, with a superposition of glucose and water absorption spectrum. The other laser has a fixed wavelength at 5.4 μm, and serves as a reference. The lasers were operated in pulse mode with repetition rate from 25 to 50 kHz; the pulse width ranged from 200 to 400 ns. The pulse peak power was from 5 to 10 mW. The duty cycle was 0.5 to 1%, and the average power was only 25 to 100 μW. A MCT photodiode (Kolmar Technologies) detector with a transimpedance amplifier (TIA) was used to measure the transmitted power.

2.2.4 *Data acquisition, signal processing, and system noise*

An automated data acquisition system was used. The computer generated a sweep of sample thickness and the transmission was measured. The signal was digitized at 40-MHz sampling rate. The overall photometric system noise was determined from three sources: laser noise, detector noise, and electronic noise. The laser RIN power spectral density was

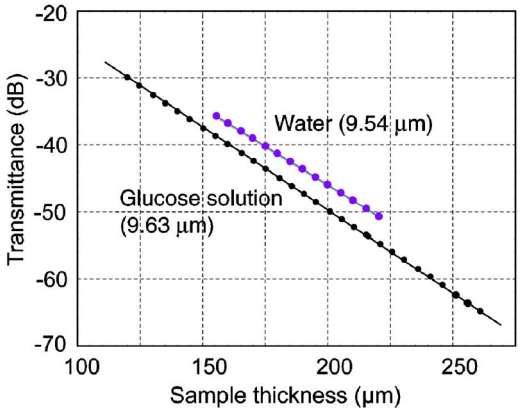

Fig. 3 Transmittance versus sample thickness, showing typical signal dynamic range of the apparatus. Upper curve actually consists of five closely spaced lines of water transmittance at 9.54-μm wavelength. The lower curve shows that of glucose at 9.63 μm.

measured to be −95 dB/Hz, which appear to be white-noise like without $1/f$ component down to 1 Hz. The combined detector and electronic noise equivalent power spectral density was measured to be ~10^{-23} W^2/Hz.

3 Experimental Results

The experimental results include: 1. demonstration of large dynamic range and sample thickness for accurate measurement of absorption coefficients μ_a, 2. calibration for specific absorption coefficient $\sigma_{a,\mathrm{glu}}$ and its accuracy, 3. the effect of IL as an interferent substance, and 4. application to the case of fixed and unknown sample optical thickness.

3.1 *System Dynamic Range and Measurements of Absorption Coefficient*

Figure 3 shows a typical transmittance that varies over 4 orders of magnitude as a function of sample thickness, which is essential for the accuracy and precision of μ_a obtained as the slope of the curve. The lower curve was for a glucose solution, and the upper curves were for pure water as a reference. The full signal range was actually over 6 orders of magnitude,[32] but only results for thickness ≥120 μm were shown. This signal dynamic range and sample thickness is much larger than those in FTIR-based works. Speed is also a figure of merit. The time for a typical scan was a few seconds, limited by the computer control and acquisition time. The actual laser on-time was only ~120 ms and its total energy was <1 mJ for the entire scan.

It appears in Fig. 3 that μ_a can be obtained via Beer's law: $\ln T = -\mu_a d$, where T is the transmittance and d the sample optical thickness. However, Beer's law is not necessarily correct, especially for laser measurements. The reason is that a focused laser beam contains many transverse components, and the effective path length is longer than the actual. Proper analysis is needed and the exact theory is given in the Appendix in Sec. 5. Deviation from Beer's law was indeed observed for a tightly focused spot and small sample thickness in this work. Calculation was performed to ensure that the results here were obtained for sufficiently large spot size and sample thickness to correctly infer the absorption coefficient.

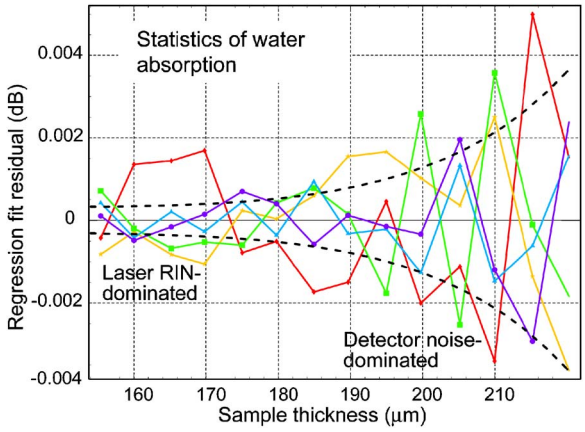

Fig. 4 Residuals of regression fit of the water transmittances shown in Fig. 3. The dashed curve shows the calculated system noise, which agrees with the observed residuals.

An example of μ_a measurement is the upper curve of Fig. 3, which actually consists of five single-scan results but are indistinguishable on this scale. The slopes yield $\mu_{a,\text{water}}$ (9.54 μm) ranging from 530.17 to 532.53 cm^{-1}, with regression standard errors (SE) varying from 0.12 to 0.29 cm^{-1}, which is $\sim$2 to 5×10^{-4} in relative terms, and the regression R^2 ranges from 0.999996 to 0.999999.

More important is the residual results shown in Fig. 4. Ideally, they should be consistent with photometric error δ as discussed in Eq. (9). Large nonrandom or systematic residuals might indicate the presence of uncontrolled variables. The residuals in Fig. 4 appear random with magnitude and behavior consistent with expected photometric system noise, which is plotted as the dashed curve in Fig. 4. It is based on the transmittance signal expressed as:

$$S=\bar{S}+\text{noise}=\bar{S}(1+\text{noise}/\bar{S})$$

$$\ln(S)-\ln(\bar{S})=\ln(1+\text{noise}/\bar{S})$$

$$\approx \text{noise}/\bar{S}=[n_{\text{det}}^2+(\bar{S}n_{\text{RIN}})^2]^{1/2}/\bar{S}, \quad (13)$$

where n_{det} and n_{RIN} are the detector noise and laser RIN, respectively. At small sample thickness, the transmitted signal is strong and the noise is dominated by laser RIN, since $\bar{S}n_{\text{RIN}}\gg n_{\text{det}}$ and the noise is

$$\sim n_{\text{RIN}}[N_{\text{RIN}}(f)\times\Delta f]^{1/2}\sim 2-3\times10^{-4},$$

where $N_{\text{RIN}}(f)$ is the laser RIN power spectral density mentioned in Sec. 2.2.4, and Δf=250 Hz is the bandwidth. At large thickness, the reverse is true: the signal is weak and dominated by detector noise. The dashed curve and data are in excellent agreement, verifying the causal relation between μ_a measurement accuracy and the basic photometry performance.

However, more extensive measurements with repeated scanning indicated another source of error unrelated to photometry. It was the mechanical variation of the sample thickness control assembly. This mechanical error was intermittent but sufficiently frequent to degrade μ_a precision to $\sim$1 to 2

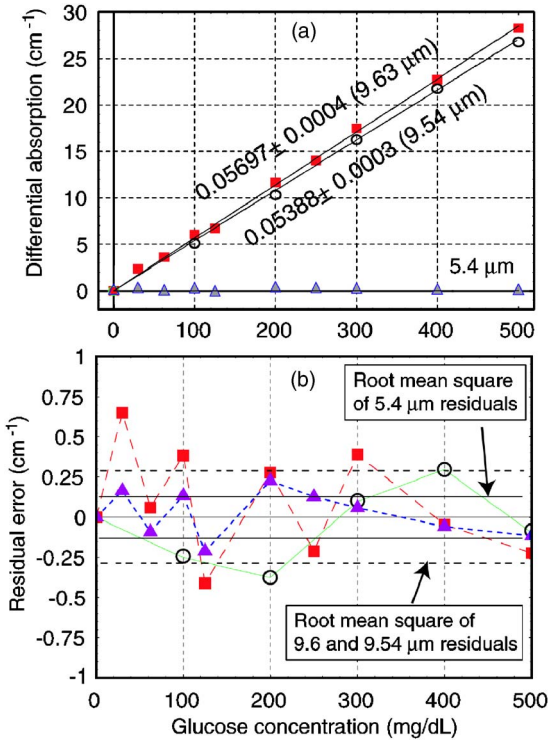

Fig. 5 (a) Absorption difference between glucose solution and DI water as a function of glucose concentration for different laser wavelengths. The regression-fit slopes are indicated in the figure. (b) The residuals of the fit along with their RMS.

$\times10^{-3}$. It could be traced to the $\sim$90-nm scan-to-scan variation of the micrometer, independently observed via interferometry. This variation was actually within the manufacturer specification of $\sim$100-nm repeatability. Another potential source of errors is the thermal expansion of the assembly, which was built on a 5-cm-long steel frame with a thermal expansion of 60 nm/K. If repeated scanning heated the frame, or room temperature varied by $\sim$1 °C, this could also contribute to errors, although evidence suggested it was less likely than the former.

Observation of this mechanical error actually underscores the importance of establishing a baseline photometric accuracy. This type of micrometer is usually adequate for many applications, but the reason for its error to be detected was because of the high sensitivity and accuracy of photometric measurements. An implication is that the full advantage of laser accuracy can be exploited for cases without moving parts or with high mechanical precision, such as microfluidic channels or optical waveguide probes.

3.2 *Specific Absorption Coefficient of Glucose (without* Intralipid®)

Calibration for specific glucose absorption coefficient $\sigma_{a,\text{glu}}$ was obtained for solutions without IL to establish the baseline glucose accuracy without interferent. It was derived from the differential absorption $\Delta\mu_{a,\text{glu}}\equiv\mu_a(C_{\text{glu}}^{\text{cal}})-\mu_a(0)$ as described by Eqs. (3)–(7). A challenge is that $\Delta\mu_{a,\text{glu}}$ is a just small difference ($\leq$6%) between two large absorption slopes, as seen in Fig. 3. Figure 5(a) shows $\Delta\mu_{a,\text{glu}}(\lambda)$ as a function of

Table 1 Regression results of differential absorption coefficients of glucose in water.

Part A - With nonlinear coefficients						
Wavelength (μm)		Coefficient	Standard error (SE)	Student t-test	$P(H_0$:coef=0)	R^2 Adjusted R^2
9.63	Linear	0.05834	0.00147	39.7	1.8×10^{-10}	0.99954
	Quadratic	-3.6×10^{-6}	3.7×10^{-6}	−0.98	0.356	0.99942
9.54	Linear	0.05288	0.00144	36.8	3.2×10^{-6}	0.99983
	Quadratic	2.4×10^{-6}	3.4×10^{-6}	0.72	0.512	0.99975
Part B - With linear coefficient only						R^2 only
9.63	Linear	0.05697	0.000433	131.5	4.4×10^{-16}	0.99948
9.54	Linear	0.05388	0.000333	161.5	1.7×10^{-10}	0.99981
5.4	Linear	0.00017	0.00018	0.945	0.369	0.09031

C_{glu} from 0 to 500 mg/dL at $\lambda=5.4$, 9.63, and 9.54 μm. The resulting regression statistics based on Eq. (3) are listed in Table 1. There are two main results: the validity of the linear model, and the accuracy of $\sigma_{a,\text{glu}}$ calibration.

The linear model discussed in Sec. 2.1 is clearly valid, as part A of Table 1 shows that the nonlinear terms ($C^2_{a,\text{glu}}$-dependency) for both the 9.63- and 9.54-μm results are insignificant, as indicated in column "$P(H_0$:coef=0)" (which indicates the probability for the null H_0 hypothesis that the nonlinear coefficient=0).

The linear regression results are shown in part B of Table 1, with $\hat{\sigma}_{a,\text{glu}}(\lambda)=5.697\times10^{-2}$ and 5.388×10^{-2} cm^{-1}/mg/dL for 9.63 and 9.54 μm, respectively. Their uncertainties are given in the SE column, which are 4.3×10^{-4} and 3.3×10^{-4} cm^{-1}/mg/dL, and in terms of relative unit, 0.76 and 0.62%. Ideally, $\hat{\sigma}_{a,\text{glu}}$ SE should be determined only by $\Delta\mu_a$ photometric error. Unfortunately, the mechanical error dominated these results. As evidenced in Fig. 5(b), the root-mean-squared (RMS) residual error of $\Delta\mu_{a,\text{glu}}(\lambda)$ is $\sim$0.29 cm^{-1} for $\lambda=9.5-9.6$ μm, which is consistent with mechanical errors for ten scan averages. The photometric error contribution should be $\sim$0.05 cm^{-1}.Without the mechanical error, the expected relative SE of $\hat{\sigma}_{a,\text{glu}}(\lambda)$ should have been $\sim1.4\times10^{-3}$ and 1.1×10^{-3}.

If this calibration is used to infer glucose concentration in unknown samples based on the simplified Eq. (8): $\hat{C}=[\hat{\sigma}_{a,\text{glu}}]^{-1}\Delta\mu_a$, the confidence level can be rigorously established based on Eq. (11), and a calculation result is shown in Fig. 6. The upper solid curves represent the confidence level for an actual worst-case mechanical error, and the lower dashed curves are for the hypothetical photometric-only error. For both, the calculation was for a single-scan error of $\Delta\mu_a$. The results show that given the mechanical error, glucose could be determined within ±21 mg/dL with 90% confidence and ±62 mg/dL with 99% confidence. For hypothetical photometry-only errors, the results would be ±6 and ±9 mg/dL for 90 and 99% confidence, respectively.

It is also clear in part B in Table 1 that the linear coefficient for 5.4 μm is within the SE, suggesting that glucose has no significant absorption at this wavelength. Thus, it can be used as a reference for samples of fixed but unknown thickness. This is further discussed in Sec. 3.4. Also evident in Fig. 5(b) is that the RMS error for $\lambda=5.4$ μm is smaller than that of 9.5 to 9.6-μm by a factor proportional to μ_a at these wavelengths, which are 233 cm^{-1} at 5.4 μm and $\sim$541 cm^{-1} at 9.6 μm. This behavior indicates that $\Delta\mu_a$ error is not a constant-amplitude additive term, but is consistent with the mechanical error, which is proportional to μ_a.

3.3 *Effect of* Intralipid® *Interference*

A matrix of samples with glucose concentration ranging from 0 to 500 mg/dL and IL concentrations from 0 to 8% were measured at $\lambda=9.63$ and 5.4 μm. The differential absorption coefficients $\Delta\mu_a$ are listed in Table 2 and plotted in Fig. 7.

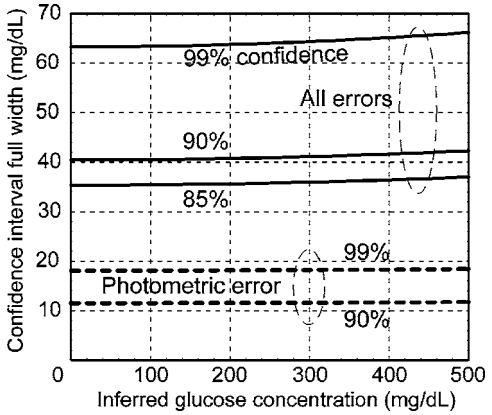

Fig. 6 Calculated confidence interval for inferred (predicted) glucose concentration. The upper solid curves are for actual errors; the lower curves are hypothetical confidence intervals if there were only photometric errors.

Table 2 Water-substracted absorption coefficients (cm^{-1}) for various glucose and Intralipid® concentrations (absorption of pure water in parentheses).

		Intralipid® concentration			
λ	Glucose concentration (mg/dL)	0%	2%	5%	8%
9.63 μm	(water μ_a:541.1 cm^{-1}) 0	0.00	−0.96	−2.92	−4.01
	100	6.08	4.8	2.67	1.65
	200	11.67	10.33	8.58	7.04
	300	17.48	15.73	14.00	12.12
	400	22.74	21.33	19.45	17.44
	500	28.26	26.57	25.43	24.34
5.4 μm	(water μ_a:233.91 cm^{-1}) 0	0.00	−7.98	−17.58	−25.88
	100	0.15	−8.30	−17.45	−26.15
	200	0.26	−8.14	−17.55	−26.24
	300	0.11	−8.18	−17.48	−26.46
	400	0.01	−8.21	−17.69	−26.35
	500	−0.03	−8.53	−17.29	−26.45

Each measurement resulted from a ten-scan average. The symbols are experimental data, and the planes are the linear regression fits. It is clear that two substances have nearly orthogonal absorption behaviors at these wavelengths. Glucose shows strong absorption at 9.63 μm, while IL has little absorption; the reverse is true at 5.4 μm. Interestingly, IL has a negative absorption coefficient at both wavelengths. This can be interpreted that the IL volume that displaces water has a lower absorption coefficient than water. Similar negative effects were reported for blood at 4.6 and 5.4 μm in a previous work.[32]

The analysis according to Eq. (7) was applied to obtain matrix $\mathbf{\Sigma}$ of Eq. (6). The main results include: 1. the validity of the linear model in Eq. (4); 2. calibration matrix $\mathbf{\Sigma}$; and 3. the effect of IL on the precision and accuracy of glucose determination.

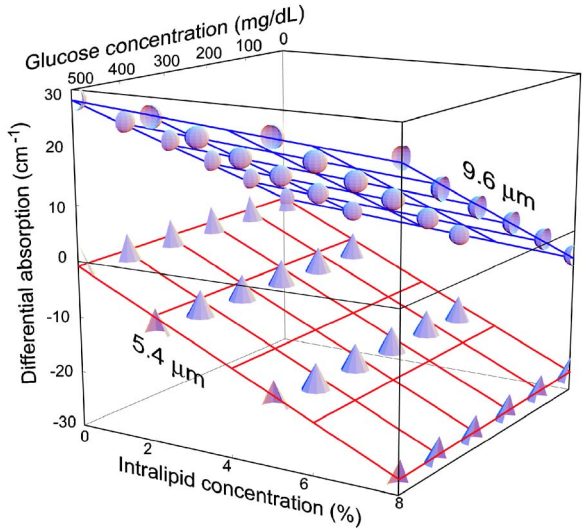

Fig. 7 Water-subtracted absorption coefficient as a function of glucose and Intralipid® concentration for two wavelengths. The symbols represent measurements, and the planes are linear regression fits.

3.3.1 *Probability of nonlinear terms*

The regression results for nonlinear terms are shown in Table 3, part A. For 9.6 μm, a *t*-test clearly shows that various nonlinear terms can be neglected. However, the results for 5.4 μm indicates a probable quadratic term for C_{IL}^2 with $P(H_0:\mathrm{coef}=0)=1.2\times10^{-8}$. This quadratic term persisted even when glucose is eliminated from the regression model, as shown in the last two rows of Table 3, part A. Further analysis, however, suggests that this nonlinear term may not be as probable as suggested by the statistics. The regression residuals for data of different glucose concentrations are not random, but systematically form clusters with respect to each value of IL concentration. A possibility for this peculiar result is that each set of samples with the same IL but different glucose concentrations were measured under similar room temperature and mechanical conditions. But sets with different IL concentrations were measured at different times and conditions, and thus had different errors. This systematic error would generate false quadratic behavior only for IL but none for glucose. Also, for both wavelengths, the cross-correlation terms $C_{\mathrm{glu}}C_{\mathrm{IL}}$ are insignificant, indicating that their absorptions are simply additive to each other.

Table 3 Regression results for glucose and Intralipid® absorptions.

Part A - With nonlinear coefficients

Wavelength (μm)		Coefficient	Standard error (SE)	Student t-test	$P(H_0: \text{coef}=0)$	R^2 Adjusted R^2
9.63	σ_{glu}	0.05772	0.00113	51.3	7.7×10^{-22}	0.99963
	σ_{IL}	−0.639	0.0737	−8.68	4.9×10^{-8}	0.99953
	$\sigma^{(2)}_{glu}$	-2.1×10^{-6}	2.5×10^{-6}	−0.821	0.422	
	$\sigma^{(2)}_{IL}$	0.0147	0.00952	1.54	0.14	
	ρ	-1.5×10^{-4}	1.1×10^{-4}	−1.39	0.18	
5.4	σ_{glu}	−0.00047	0.00122	−0.38	0.706	0.99960
	σ_{IL}	−4.035	0.0802	−50.3	1.1×10^{-21}	0.99950
	$\sigma^{(2)}_{glu}$	2.8×10^{-7}	2.7×10^{-6}	0.1	0.919	
	$\sigma^{(2)}_{IL}$	0.0986	0.0104	9.52	1.2×10^{-8}	
	ρ	-4×10^{-5}	1.2×10^{-4}	−0.335	0.741	
5.4	σ_{IL}	−4.087	0.06354	−64.3	1.53×10^{-26}	0.99957
	$\sigma^{(2)}_{IL}$	0.1024	0.0089	−11.5	8.9×10^{-11}	0.99953

Part B - With linear coefficient only

Wavelength (μm)		Coefficient	Standard error (SE)	Student t-test	$P(H_0: \text{coef}=0)$	R^2 Adjusted R^2
9.63	σ_{glu}	0.05632	0.000305	184.5	1.4×10^{-36}	0.99954
	σ_{IL}	−0.5500	0.0192	−28.7	6.3×10^{-19}	0.99950

ANOVA

	Degree of freedom	Sum of square	Mean of square	F ratio	$P(H_0: \text{coef}=0)$
Model	2	5753	2876.47	23871	2×10^{-37}
Error	22	2.651	0.1205		
Total	24	5756			

Covariance matrix $10^{-4}\times\begin{bmatrix} 9.3\times10^{-4} & -0.038 \\ -0.038 & 3.68 \end{bmatrix}$

5.4	σ_{glu}	−0.00169	0.000742	−2.28	0.033	0.99755
	σ_{IL}	−3.3084	0.0466	−71	1.7×10^{-27}	0.99732

ANOVA

	Degree of freedom	Sum of square	Mean of square	F ratio	$P(H_0: \text{coef}=0)$
Model	2	6366	3183	4472	1.9×10^{-29}
Error	22	15.7	0.712		
Total	24	6381			

Covariance matrix $10^{-3}\begin{bmatrix} 5.5\times10^{-4} & -0.022 \\ -0.022 & 2.17 \end{bmatrix}$

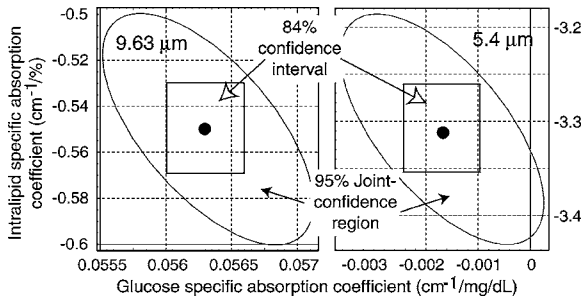

Fig. 8 Specific absorption coefficients of glucose and Intralipid® for 9.63 μm (left) and 5.4 μm (right) from regressions of measurements in Fig. 7. The ellipses represent the 95%-joint-confidence region; the rectangles represent the 84%-confidence interval of each coefficient.

3.3.2 *Linear coefficients*

With the nonlinear terms excluded, the linear regression results are shown in Table 3, part B. For both, the F-ratio statistics indicated that the linear model alone was quite sufficient to account for the data. The coefficients $\hat{\sigma}_{a,\mathrm{glu}}(\lambda)$ and $\hat{\sigma}_{a,\mathrm{IL}}(\lambda)$ along with the contour of 95% joint-confidence ellipse (based on F-ratio distribution) and individual 84% confidential intervals (based on t-distribution) are plotted in Fig. 8. For 9.63 μm, the $\hat{\sigma}_{a,\mathrm{glu}}$ value of 0.0563 $\mathrm{cm}^{-1}/\mathrm{mg/dL}$ is comparable to the value 0.05697 for no-IL obtained in Sec. 3.2. For 5.4 μm, $\hat{\sigma}_{a,\mathrm{glu}}$ is clearly not significant.

3.3.3 *Inferred glucose and intralipid concentration*

With calibrated coefficients $\mathbf{\Sigma}$, the reverse inference of glucose and IL concentration can be obtained via Eq. (8). There was no need to prepare unknown samples given the available extensive number of samples. The results are shown in Fig. 9. The filled circles represent known values, the open squares with center dots represent inferred values. The residuals of all 24 concentrations are shown in the scatter plot of Fig. 10.

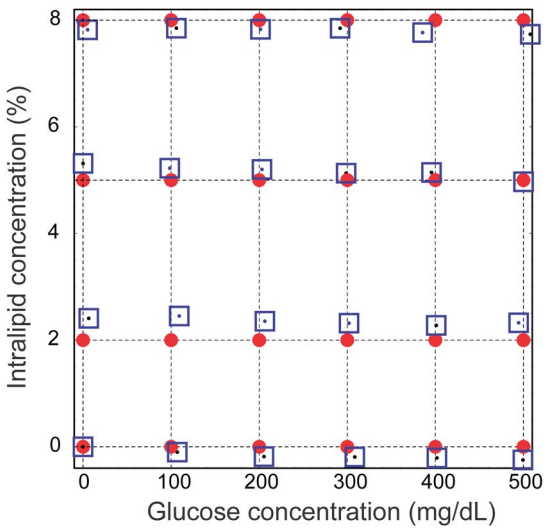

Fig. 9 Inferred concentrations of glucose and Intralipid® (open square symbols with a dot in the center) versus their known values (filled circles) for the 24 samples.

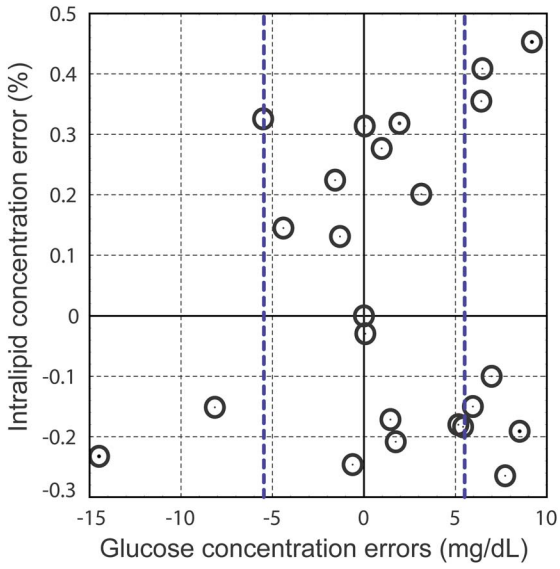

Fig. 10 Discrepancies of inferred concentrations versus known values for glucose and Intralipid® shown in Fig. 9. The vertical dashed lines represent the root mean square of glucose errors.

It appears from Figs. 9 and 10 that the residuals of IL concentration do not seem to be random around the expected values. All inferred IL concentrations in Fig. 9 are either higher or lower than expected values, forming two distinctive clusters in Fig. 10. This reflects the systematic error discussed before for the 5.4-μm IL data.

More important are the glucose results. The RMS of all residual glucose errors shown in Fig. 10 is 5.7 mg/dL, indicated by the two thick dashed lines. Figure 11 plots the glucose RMS error for each IL. Here, the result in Sec. 3.2 is just a subset with C_{IL}=0%. These RMS errors are consistent with the mechanical errors, and there is no obvious correlation between glucose RMS and C_{IL}, indicating that IL has no effect on glucose error. The result is hardly surprising, considering that the two substances have orthogonal absorption behaviors at the two wavelengths.

Ellipsoid confidence contours can be calculated for inferred glucose and IL concentrations; however, they are not

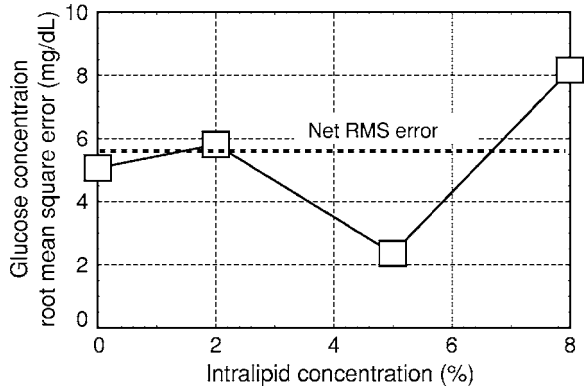

Fig. 11 Glucose concentration errors versus Intralipid® concentration show no discernible trend. In other words, IL does not affect glucose measurement accuracy.

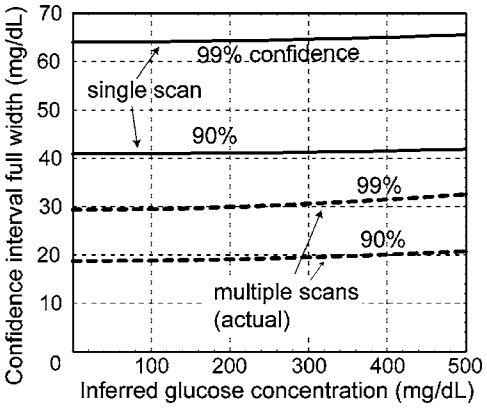

Fig. 12 Calculated confidence interval for inferred glucose concentration with an arbitrary IL concentration between 0 to 8%. The upper solid curves are for a single scan; the lower curves are for a ten-scan average.

relevant with regard to IL, owing to the IL systematic errors, and IL is also not of interest. Therefore, the bivariate PDF $P(\mathbf{C} \equiv \{C_{\text{glu}}, C_{\text{IL}}\})$ can be integrated over C_{IL} to yield PDF for C_{glu} only, and numerical approximation can be used to obtain the confidence interval. The result is shown in Fig. 12. It is remarkably similar to the result without IL in Fig. 6, confirming that IL does not interfere with glucose accuracy. Comparison of Figs. 12 and 10 shows that all 24 glucose data points fall within the calculated 99% confidence level, and 23 out of 24 (96%) fall within the calculated 90% confidence level.

3.4 *Approach for Fixed and Unknown Thickness*

In applications such as monitoring a microfluidic channel, microassay array, or diffuse scattering from tissues, the sample effective optical thickness d is usually fixed or unknown. The system must infer the concentrations without varying the thickness. For these cases, the algorithm is slightly modified from that in Sec. 2.1 by treating d as an additional unknown variable. The details are described in Appendix B in Sec. 6. The essential result is similar to Eq. (8):

$$\hat{\mathbf{C}}_X = -(\mathbf{\Sigma}_X^{\mathrm{T}}\mathbf{\Sigma}_X)^{-1}\mathbf{\Sigma}_X^{\mathrm{T}} \cdot \ln \mathbf{S}, \tag{14}$$

where $\hat{\mathbf{C}}_X$ is modified from $\hat{\mathbf{C}}$ by including d, $\mathbf{\Sigma}_X$ is modified by including water absorption, and a key difference is to use $\ln \mathbf{S}$ instead of $\Delta\boldsymbol{\mu}_a$, where $\mathbf{S}$ is the optical signal that can be transmission or backscattering.

It is sufficient to consider an example to illustrate the principle, and this is summarized in Table 4. The first two rows show the numerical values of $\mathbf{\Sigma}_X$, $(\mathbf{\Sigma}_X^{\mathrm{T}}\mathbf{\Sigma}_X)^{-1}$ and $\ln \mathbf{S}(\lambda)$, which are obtained from the transmittance data of an aqueous glucose sample set at a fixed assembly thickness. The last two rows show inferred value $\hat{d} = 150.6\ \mu$m and $\hat{C}_{\text{glu}} = 570$ mg/dL, to be compared with known values 150 μm and 500 mg/dL, respectively. There is good agreement for $\hat{d}$, but $\hat{C}_{\text{glu}}$ is a bit off, which is likely due to some unaccounted optical loss (Appendix B in Sec. 6.).

A crucial aspect of this result is the choice of wavelengths. A requirement of Eq. (14) is that $(\mathbf{\Sigma}_X^{\mathrm{T}}\mathbf{\Sigma}_X)^{-1}$ is not badly conditioned, which in principle is no different from Eq. (8). In practice, however, it is a more critical requirement, since $\mathbf{\Sigma}_X$ contains $\mu_{a,\text{water}}(\lambda)$, which provides spectral contrast to infer d. Since $\mu_{a,\text{water}}(\lambda)$ is large, the λ's must be chosen such that $\mu_{a,\text{water}}(\lambda)$ has variation much larger than their uncertainty. In the second row of Table 4, the small-font numbers for $(\mathbf{\Sigma}_X^{\mathrm{T}}\mathbf{\Sigma}_X)^{-1}$ indicate its uncertainty. Their small uncertainty values ensure that $(\mathbf{\Sigma}_X^{\mathrm{T}}\mathbf{\Sigma}_X)^{-1}$ is meaningful, owing to the large water absorption difference between 5.4 and 9.6 μm. In comparison, any wavelength set in the laser tuning range 9.5 to 9.8 μm was not as useful, since water absorption varies too slowly over this range. Both this and the IL results suggest that large wavelength diversity can be advantageous for accuracy and confidence, as discussed in Appendix B Sec. 6.

Table 4 Example of inferring unknown optical thickness.

$\lambda_1 = 5.4\ \mu$m, $\lambda_2 = 9.63\ \mu$m

$\mathbf{\Sigma}_X = \begin{pmatrix} \mu_{a,w}(\lambda_1) & \sigma_{a,\text{glu}}(\lambda_1) \\ \mu_{a,w}(\lambda_2) & \sigma_{a,\text{glu}}(\lambda_2) \end{pmatrix}$	$(\mathbf{\Sigma}_X^T\mathbf{\Sigma}_X)^{-1}$	$\ln \mathbf{S}(\lambda)$
$\begin{pmatrix} 233.91 & 0.17 \\ 541.1 & 56.97 \end{pmatrix}$	$10^{-3} \times \begin{pmatrix} 0.0185 & -0.176 \\ \pm 3.9 \times 10^{-4} & \pm 5 \times 10^{-2} \\ -0.176 & 1.98 \\ \pm 5 \times 10^{-2} & \pm 0.07 \end{pmatrix}$	$\begin{pmatrix} -3.523 \\ -8.635 \end{pmatrix}$

$$\begin{pmatrix} \hat{d} \\ \hat{C}_{\text{glu}}\hat{d} \end{pmatrix} = -(\mathbf{\Sigma}_X^T\mathbf{\Sigma}_X)^{-1}\mathbf{\Sigma}_X^T \ln \mathbf{S} = \begin{pmatrix} 0.01506 \\ 0.008578 \end{pmatrix}$$

With proper unit conversion

$$\begin{pmatrix} \hat{d} \\ \hat{C}_{\text{glu}} \end{pmatrix} = \begin{pmatrix} 150.6\ \mu\text{m} \\ 570\ \text{mg/dL} \end{pmatrix}; \begin{pmatrix} d \\ C_{\text{glu}} \end{pmatrix} = \begin{pmatrix} 150\ \mu\text{m} \\ 500\ \text{mg/dL} \end{pmatrix}$$

4 Summary and Conclusion

This work describes the use of mid-IR semiconductor lasers to measure aqueous glucose concentration and examines the issue of accuracy. Compared with many previous works[7–14] that focused mainly on spectroscopy, this work aims at photometric engineering to demonstrate the merit of the laser-based technique as opposed to others such as FTIR. Specifically, the work focuses on the laser properties of high signal-to-noise ratio, large dynamic range, and speed. The laser capability to focus onto a small sample volume ($\sim 4 \times 10^{-7}$ mL) is also suitable for microfluidic and microarray bioassay applications.

The approach measures the absorption coefficients of aqueous glucose and Intralipid® solutions of various concentrations for different wavelengths (5.4, 9.54, and 9.63 μm). Linear regression is applied to obtain the specific absorption coefficients for each solute, which are then applied to infer their concentrations and compare with known values.

The important issue is accuracy, and the errors are shown to be causally and deterministically related to the basic instrument noises and system errors. There are no unaccounted sources of error. This causal relation allows inferring measurement confidence level based on rigorous system understanding instead of phenomenological assessment. The results show that glucose concentration could be determined ±21 and ±32 mg/dL with 90 and 99% confidence, respectively, in a single measurement. These values improve to ±9.5 and ±15 mg/dL with ten measurements. These uncertainties were not limited by photometry, but by a larger mechanical error of the sample thickness control assembly. This mechanical error is not fundamental, and in applications without this problem, the expected uncertainty due to photometry-only error would be ±6 and ±9 mg/dL for 90 and 99% confidence level, respectively, for a single measurement. Intralipid® up to 8% concentration had no effect on the glucose measurement.

The choice of wavelengths is also evidently important. The large difference between 5.4 and 9.63 μm offers large spectral contrast between glucose, IL, and water that contributes to the measurement confidence. In general, for the laser method, fewer λ's entails a simpler system, whereas FTIR offers the entire spectrum. However, an insight from these results is that with regard to accuracy, measurements with many wavelengths but noisy is not necessarily better than those with fewer wavelengths but low noise. Other recent MIR works[10–13,24] even with FTIR also suggest that a few wavelengths might be sufficient. The laser approach can thus be applicable and practical.

5 Appendix A: Deviation from Beer's Law for Focused Laser Beam

In transmission or diffuse backscattering, the laser light coherence property may require the full optical solution for accurate interpretation of the result. For an absorptive thin film with parallel interfaces, i.e., a lossy etalon, the transmittance is:

$$t_{\mathrm{TE}} = \{1 + [1 - \exp(2idk_2)](k_1 - k_2)^2/4k_1k_2\}^{-1}\exp(idk_2)$$

$$t_{\mathrm{TM}} = \{1 + [1 - \exp(2idk_2)] \times (\varepsilon_2 k_1 - \varepsilon_1 k_2)^2/4\varepsilon_1\varepsilon_2 k_1 k_2\}^{-1}\exp(idk_2) \quad (15)$$

where TE and TM denote the transverse electric and magnetic polarization, respectively, and d is the sample thickness. For all other quantities, the subscripts 1 and 2 correspond to the window and sample, respectively. $\varepsilon \equiv (n+i\kappa)^2$ is the complex dielectric constant; $k = \sqrt{\varepsilon k_0^2 - \beta^2}$ with $k_0 = 2\pi/\lambda$, and β is the transverse wave number of the beam parallel to the interface.

For small β, the paraxial approximation can be used:

$$k = \sqrt{\varepsilon k_0^2 - \beta^2} \approx \sqrt{\varepsilon} k_0 \left(1 - \frac{\beta^2}{2\varepsilon k_0^2}\right) \approx (n + i\kappa)k_0 - \frac{\beta^2}{2nk_0}\left(1 - i\frac{\kappa}{n}\right), \quad (16)$$

$$k \approx nk_0\left(1 - \frac{\beta^2}{2n^2k_0^2}\right) + i\kappa k_0\left(1 + \frac{\beta^2}{2n^2k_0^2}\right) \approx nk_0\cos\theta + i\kappa k_0\frac{1}{\cos\theta}, \quad (17)$$

where θ is the beam propagation angle in the medium. Substituting the imaginary component in $\exp(idk_2)$ of Eq. (15) results in the absorption term:

$$\exp(-d\kappa k_0)\frac{1}{\cos\theta} = \exp\left(-\frac{1}{2}\mu_a d\frac{1}{\cos\theta}\right); \quad (\mu_a \equiv 2\kappa k_0), \quad (18)$$

which indicates that the beam experiences a larger loss factor $1/\cos\theta$ associated with a longer path length. A focused laser beam is a superposition of many plane waves with nonvanishing transverse β, therefore it experiences a higher loss than a normal-incident plane wave.

In this work, the index of refraction of the CaF_2 window is very close to that of water, and there is little difference between TE and TM transmissions. Thus the net beam transmittance is:

$$T = \int\int d\beta_x d\beta_y A(\beta_x)A(\beta_y)|t_{\mathrm{TE}}|^2, \quad (19)$$

where $A(\beta_x)$, $A(\beta_y)$ are the power spectral density functions of transverse spatial frequencies β_x, β_y. For an x-y Gaussian beam:

$$A(\beta) = \frac{w}{\sqrt{2\pi}}\exp(-w^2\beta^2/2). \quad (20)$$

With paraxial approximation, applying Eq. (19) with Eq. (20) yields:

$$T = \exp(-\mu_a d)\frac{w_x}{(w_x^2 + \mu_a d/k_0^2 n_2^2)^{1/2}}\frac{w_y}{(w_y^2 + \mu_a d/k_0^2 n_2^2)^{1/2}}, \quad \text{and} \quad (21)$$

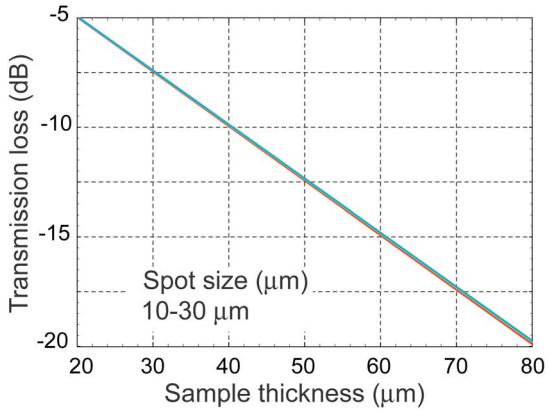

Fig. 13 Numerical calculation of transmission loss (transmittance) of a semiconductor laser beam with different spot sizes (ranging from 10 to 30 μm) as a function of sample thickness. The small differences between them are more visible in Fig. 14.

$$T \approx \exp(-\mu_a d)\frac{k_0^2 n_2^2 w_x w_y}{\mu_a d} \text{ for small } w_x, w_y. \qquad (22)$$

From Eq. (21), Beer's law would be obtained for large beam waists: w_x^2, $w_y^2 \gg \mu_a d/k_0^2 n_2^2 (=\mu_a d\lambda^2/4\pi^2 n_2^2)$. But for small beam waists, Eq. (22) shows a deviation by the term $k_0^2 n_2^2 w_x w_y/\mu_a d$, which would lead to substantial error of μ_a if not included.

In this work, the semiconductor laser beam is not Gaussian and has x-y asymmetry. A numerical calculation for a modeled laser beam produces results shown in Figs. 13–15. Figure 13 shows that the transmittance is superficially similar to Beer's law on a large scale. But as evidenced in Fig. 14, the residuals from the exponential fit clearly deviate from Beer's law, even if the interference fringes are ignored. The deviation is worse for smaller spot size as expected. The "effective" absorption coefficient deviates from the actual coefficient as

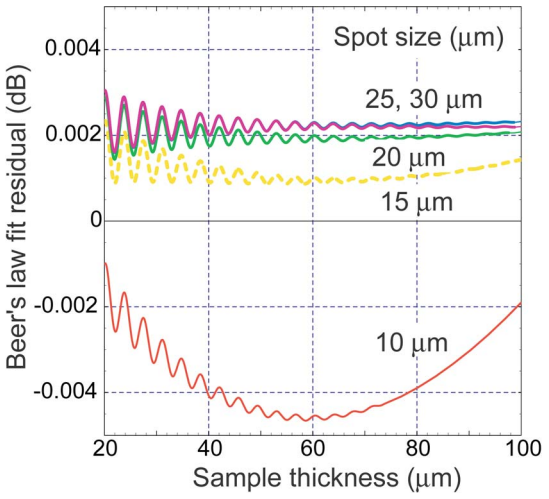

Fig. 14 Residual of fits of the transmittance curves in Fig. 13 with Beer's law, showing clear deviation from the law for small laser spot sizes. The oscillations are simply the interference fringes.

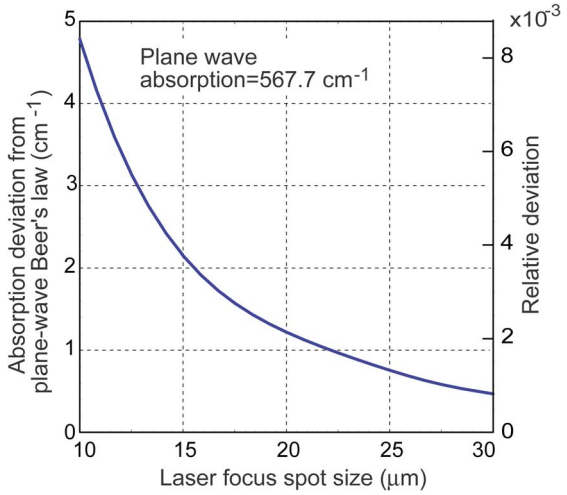

Fig. 15 Errors of absorption coefficient if Beer's law is applied to the results in Fig. 13. Smaller laser spot size results in larger errors, which can be as much as 0.8% in this case.

shown in Fig. 15. Considering that the largest differential glucose absorption is only ~28.5 cm^{-1} in this work, a deviation of 4 cm^{-1} would result in an error of 14%.

This error does not just occur on the slope of the log transmittance, but also on its amplitude. Thus, for cases with fixed-thickness samples, the error on transmittance amplitude is similarly as severe and correction is necessary.

6 Appendix B: Approach for Fixed or Unknown Sample Effective Optical Thickness

In general, the transmission or diffuse backscattered return signal can be expressed as:

$$S(\lambda) = Q(\lambda)\exp[-\mu_a(\lambda)d], \qquad (23)$$

where $Q(\lambda)$ is a loss factor that may or may not be known, and $\mu_a(\lambda)$ is a sum of absorptions:

$$\ln S(\lambda) = -\mu_{a,w}(\lambda)d - \sum_{i=1}^{k} \sigma_{a,i}(\lambda)C_i d + \eta(\lambda), \qquad (24)$$

where $\eta(\lambda) \equiv \ln Q(\lambda)$, $\mu_{a,w}(\lambda)$ is the baseline absorption coefficient of the medium (which can be a solvent other than water), d can represent single or round-trip, and C_i for $i=1$ to k denotes concentration of substance of interest.

In controlled applications with fixed, known d and η, Eq. (24) can be written:

$$\frac{1}{d}\begin{Bmatrix}\eta(\lambda_1)-\ln[S(\lambda_1)]\\ \eta(\lambda_2)-\ln[S(\lambda_2)]\\ \vdots\\ \eta(\lambda_n)-\ln[S(\lambda_n)]\end{Bmatrix}-\begin{bmatrix}\mu_{a,w}(\lambda_1)\\ \mu_{a,w}(\lambda_2)\\ \vdots\\ \mu_{a,w}(\lambda_m)\end{bmatrix}$$
$$=\begin{bmatrix}\sigma_{a,1}(\lambda_1) & \sigma_{a,2}(\lambda_1) & \cdots & \sigma_{a,k}(\lambda_1)\\ \sigma_{a,1}(\lambda_2) & \sigma_{a,2}(\lambda_2) & \cdots & \sigma_{a,k}(\lambda_2)\\ \vdots & \vdots & \ddots & \vdots\\ \sigma_{a,1}(\lambda_n) & \sigma_{a,2}(\lambda_n) & \cdots & \sigma_{a,k}(\lambda_n)\end{bmatrix}\begin{pmatrix}C_1\\ C_2\\ \vdots\\ C_k\end{pmatrix}, \quad (25)$$

and a solution similar to Eq. (8) is obtained:

$$\hat{\mathbf{C}}=(\mathbf{\Sigma}^{\mathrm{T}}\mathbf{\Sigma})^{-1}\mathbf{\Sigma}^{\mathrm{T}}\cdot\left[\frac{1}{d}(\boldsymbol{\eta}-\ln\mathbf{S})-\boldsymbol{\mu}_{a,w}\right]. \quad (26)$$

If d is unknown, Eq. (24) can be written:

$$\begin{Bmatrix}\eta(\lambda_1)-\ln[S(\lambda_1)]\\ \eta(\lambda_2)-\ln[S(\lambda_2)]\\ \vdots\\ \eta(\lambda_n)-\ln[S(\lambda_n)]\end{Bmatrix}$$
$$=\begin{bmatrix}\mu_{a,w}(\lambda_1) & \sigma_{a,w}(\lambda_1) & \sigma_{a,1}(\lambda_1) & \cdots & \sigma_{a,k}(\lambda_1)\\ \mu_{a,w}(\lambda_2) & \sigma_{a,w}(\lambda_2) & \sigma_{a,2}(\lambda_2) & \cdots & \sigma_{a,k}(\lambda_2)\\ \vdots & \vdots & \vdots & \ddots & \vdots\\ \mu_{a,w}(\lambda_n) & \sigma_{a,w}(\lambda_n) & \sigma_{a,1}(\lambda_n) & \cdots & \sigma_{a,k}(\lambda_n)\end{bmatrix}\times\begin{pmatrix}d\\ C_1d\\ \vdots\\ C_kd\end{pmatrix}. \quad (27)$$

If η is negligible, Eq. (27) leads to Eq. (14). If η is unknown, the problem cannot be solved. However, $\eta(\lambda)$ usually represents optics effects such as light collection loss, Fresnel loss, scattering loss, or chromatic dispersion, and therefore can be a slowly varying function of wavelength. For the sake of discussion, suppose that it can be parametrized to the first order:

$$\eta(\lambda)=\eta_0+\rho_1\lambda, \quad (28)$$

then Eq. (27) can be modified to yield:

$$\begin{Bmatrix}\ln[S(\lambda_1)]\\ \ln[S(\lambda_2)]\\ \vdots\\ \ln[S(\lambda_n)]\end{Bmatrix}$$
$$=-\begin{bmatrix}\mu_{a,w}(\lambda_1) & \sigma_{a,1}(\lambda_1) & \cdots & \sigma_{a,k}(\lambda_1) & -\lambda_1 & -1\\ \mu_{a,w}(\lambda_2) & \sigma_{a,1}(\lambda_2) & \cdots & \sigma_{a,k}(\lambda_2) & -\lambda_2 & -1\\ \vdots & \vdots & \ddots & \vdots & \vdots & \vdots\\ \mu_{a,w}(\lambda_n) & \sigma_{a,1}(\lambda_n) & \cdots & \sigma_{a,k}(\lambda_n) & -\lambda_n & -1\end{bmatrix}\times\begin{pmatrix}d\\ C_1d\\ \vdots\\ C_kd\\ \rho_1\\ \eta_0\end{pmatrix}, \quad (29)$$

which allows inferring all three unknown parameters d, η_0, and ρ_1.

A crucial requirement relevant to the wavelengths used in this work is that $(\mathbf{\Sigma}_X^T\mathbf{\Sigma}_X)^{-1}$ should have low uncertainty. Let each row or column of $\mathbf{\Sigma}_X$ be denoted as a vector $\mathbf{s}$. If the wavelength range is too narrow, various vector $\mathbf{s}_i$ can become close to each other, $(\mathbf{\Sigma}_X^T\mathbf{\Sigma}_X)^{-1}$ can be nearly degenerate with large uncertainty, and the measurements would have poor confidence. A nominal criterion for the vectors to be "far" from each other is to use the quasi-Mahalanobis distance:

$$\min\left[\frac{\|\mathbf{s}_i-\gamma\mathbf{s}_j\|}{u\sqrt{2}},\ \forall\ \gamma\right]$$
$$\equiv\min\left(\sqrt{\left\{\sum_{p=1}^{r}\frac{[s_{ip}-\gamma s_{jp}]^2}{u^2(s_{ip})+\gamma^2u^2(s_{jp})}\right\}^{1/2}},\ \forall\ \gamma\right)\gg 1, \quad (30)$$

where m_{xp} are the vector elements, $u^2(s_{xp})$ are their uncertainties, and γ is a proportional factor.

Applying this criterion in this case explains the reason why the 5.4- and 9.6-μm wavelength combination produced the best results in Sec. 3.4. The quasi-Mahalanobis distance for $\mathbf{\Sigma}_X$ columns with 5.4 and 9.63 μm is 93, compared to only ~3.5 to 6 for any set of wavelengths in the 9.5 to 9.8-μm range.

Acknowledgment

This work was supported in part by the DARPA/ARO under contract DAAD-190010361, the Air Force Research Laboratory under contract F29601-00-2-0058, and the State of Texas through the THECB and the Texas Center for Advanced Materials and Center for Superconductivity. We thank the late Pradeep Johnson, C. Peng, G. P. Luo, and A. Seetheraman for valuable assistance.

References

1. See http://www.diabetes.org/about-diabetes.jsp.
2. C. M. Peterson, "*Diabetes Management in the '80s: The Role of Home Blood Glucose Monitoring and New Insulin Delivery Systems*," Praeger, New York (1982).
3. M. Rohrscheib, R. Robinson, and R. Philip Eaton, "Non-invasive glucose sensors and improved informatics—the future of diabetes management," *Diabetes, Obesity Metabolism* **5**(5), 280–281 (2003).
4. D. C. Klonoff, "Noninvasive blood glucose monitoring," *Diabetes Care* **20**(3), 433–437 (1997).
5. O. S. Khalil, "Spectroscopic and clinical aspects of noninvasive glucose measurements," *Clin. Chem.* **45**, 165–177 (1999).
6. G. Cote, "Non-invasive and minimally invasive optical monitoring technologies," *J. Nutr.* **131**, 1596S–1604S (2001).
7. H. M. Heise, R. Marbach, G. Janatsch, and J. D. Kruse-Jarres "Multivariate determination of glucose in whole blood by attenuated total reflection infrared spectroscopy," *Anal. Chem.* **61**, 2009–2015 (1989).
8. D. M. Haaland, "Multivariate calibration methods applied to quantitative FT-IR analysis," in *Practical Fourier Transform Infrared Spectroscopy*, J. R. Ferraro and K. Krishnan, Eds., pp. 395–486, Academic Press, New York (1990).
9. P. Bhandare, Y. Mendelson, E. Stohr, and R. A. Peura "Glucose determination in simulated plasma blood serum solutions by FTIR spectroscopy: investigation of spectral interferences," *Vib. Spectrosc.* **6**, 363–378 (1994).
10. R. Vonach, J. Buschmann, R. Falkowski, R. Schindler, B. Lendl, and R. Keller, "Application of mid-infrared transmission spectrometry to the direct determination of glucose in whole blood," *Appl. Spectrosc.* **52**, 820–822 (1998).

11. Y. C. Shen, A. G. Davies, E. H. Linfield, T. S. Elsey, P. F. Taday, and D. D. Arnone, "The use of Fourier-transform infrared spectroscopy for the quantitative determination of glucose concentration in whole blood," *Phys. Med. Biol.* **48**(13), 2023–2032 (2003).
12. Y. J. Kim, S. Hahn, and G. Yoon, "Determination of glucose in whole blood samples by mid-infrared spectroscopy," *Appl. Opt.* **42**(4), 745–749 (2003).
13. W. B. Martin, S. Mirov, and R. Venugopalan, "Using two discrete frequencies within the middle infrared to quantitatively determine glucose in serum," *J. Biomed. Opt.* **7**(4), 613–617 (2002).
14. M. Rhiel, P. Ducommun, I. Bolzonella, I. Marison, and U. von Stockar, "Real-time in situ monitoring of freely suspended and immobilized cell cultures based on mid-infrared spectroscopic measurements," *Biotechnol. Bioeng.* **77**(2), 174–185 (2002).
15. C. D. Malchoff, K. Shoukri, J. I. Landau, and J. M. Buchert, "A novel noninvasive blood glucose monitor," *Diabetes Care* **25**, 2268–2275 (2002).
16. M. A. Arnold, "Non-invasive glucose monitoring," *Curr. Opin. Biotechnol.* **7**(1), 46–49 (1996).
17. M. A. Arnold and C. W. Small, "Noninvasive glucose sensing," *Anal. Chem.* **77**(17), 5429–5439 (2005).
18. J. W. Hall and A. Pollard, "Near-infrared spectrophotometry: a new dimension in clinical chemistry," *Clin. Chem.* **38**(9), 1623–1631 (1992).
19. M. R. Robinson, R. P. Eaton, D. M. Haaland, G. W. Koepp, E. V. Thomas, B. R. Stallard, and P. L. Robinson, "Noninvasive glucose monitoring in diabetic patients: a preliminary evaluation," *Clin. Chem.* **38**(9), 1618–1622 (1992).
20. H. M. Heise, R. Marbach, T. Koschinsky, and F. A. Gries, "Noninvasive blood glucose sensors based on near-infrared spectroscopy," *Artif. Organs* **18**(6), 439–447 (1994).
21. R. Marbach, T. H. Koschinsky, F. A. Gries, and H. M. Heise, "Noninvasive blood glucose assay by near-infrared diffuse reflectance spectroscopy of the human inner lip," *Appl. Spectrosc.* **47**, 875–881 (1993).
22. V. Saptari and K. Youcef-Toumi, "Design of a mechanical-tunable filter spectrometer for noninvasive glucose measurement," *Appl. Opt.* **43**(13), 2080–2088 (2004).
23. M. J. McShane and G. L. Cote', "Near-infrared spectroscopy for determination of glucose, lactate, and ammonia in cell culture media," *Appl. Spectrosc.* **52**, 1073–1078 (1998).
24. J. Burd (Private communication).
25. K. M. Quan, G. B. Christison, H. A. MacKenzie, and P. Hodgson, "Glucose determination by a pulsed photoacoustic technique: an experimental study using a gelatin-based tissue phantom," *Phys. Med. Biol.* **38**, 1911–1922 (1993).
26. Y. Shen, Z. Lu, S. Spiers, H. A. MacKenzie, H. S. Ashton, J. Hannigan, S. S. Freeborn, and J. Lindberg, "Measurement of the optical absorption coefficient of a liquid by use of a time-resolved photoacoustic technique," *Appl. Opt.* **39**, 4007–4012 (2000).
27. B. Guo, Y. Wang, C. Peng, G. Luo, and H. Q. Le, "Multi-wavelength mid-infrared micro-spectral imaging using semiconductor lasers." *Appl. Spectrosc.* **57**, 811–822 (2003).
28. G. P. Luo, C. Peng, H. Q. Le, S. S. Pei, W. Y. Hwang, B. Ishaug, J. Um, J. N. Baillargeon, and C. H. Lin, "Grating-tuned external-cavity quantum cascade semiconductor lasers," *Appl. Phys. Lett.* **78**, 2834–2836 (2001).
29. G. Luo, C. Peng, H. Q. Le, S. S. Pei, H. Lee, W. Y. Hwang, and B. J. Zheng, "Broadly wavelength-tunable external cavity mid-infrared quantum cascade lasers," *IEEE J. Quantum Electron.* **38**, 931 (2002).
30. C. Peng, G. P. Luo, and H. Q. Le, "Broadband, continuous, and fine-tuning properties of external-cavity TE-stabilized mid-IR quantum cascade laser," *Appl. Opt.* **42**, 4877–4882 (2003).
31. C. Peng, H. L. Zhang, and H. Q. Le, "Mid-infrared external-cavity two-segment quantum cascade laser," *Appl. Phys. Lett.* **83**, 4098–4100 (2003).
32. B. Guo, Y. Wang, C. Peng, H. L. Zhang, G. P. Luo, H. Q. Le, C. Gmachl, D. L. Sivco, M. L. Peabody, and A. Y. Cho, "Laser-based mid-infrared reflectance imaging of biological tissues," *Opt. Express* **12**, 208 (2004).